Control of Chaos in Atomic Force Microscopes [1]

M. Ashhab,   M.V. Salapaka,   M. Dahleh   and   I. Mezić

Mechanical and Environmental Engineering Dept.

University of California at Santa Barbara

CA 93106

Abstract

In this paper, we study the dynamical behaviour of
a microcantilever-sample system that forms the basis
for the operation of atomic force microscopes (AFM).
We model the micro-cantilever by a single mode ap-
proximation and the interaction between the sample
and cantilever by a van der Waals (vdW) potential.
The cantilver is vibrated by a sinusoidal input, and
its deflection is detected optically. We analyze the
forced dynamics using Melnikov method, which re-
veals the region in the space of physical parameters
where chaotic motion is possible. In addition, using
a proportional and derivative controller we compute
the Melnikov function in terms of the parameters of
the controller. Using this relation it is possible to
design controllers that will remove the possibility of
chaos.

1. Introduction

Surfaces at the atomic level can be probed with good
accuracy using the atomic force microscope (AFM)
which was invented in 1986. This is done by moving
the sample beneath a tip attached to a soft cantilever
which causes the cantilever to deflect. The cantilever
deflection is measured by optical methods and is used
as an indicator of the force variation on the sample.
The behaviour of the cantilever depends on the inter-
action force between its tip and the sample, the spring
force which is due to the cantilever, and the equilib-
rium position of the tip in the absence of the inter-
action forces. Many cantilever-based instruments are
now available which can be used for force measure-
ments, magnetic spin detection, and thermal mea-
surements [5]. All of these instruments share this ba-
sic mechanism of a micro-cantilever interacting with
a sample.

It has been experimentally observed that the motion
of the cantilever can be chaotic under certain phys-

ical conditions [6]. This type of irregular motion is
highly undesirable for the AFM performance since
it causes the AFM to give inaccurate measurements.
This paper is concerned with the modeling, analysis
and control of a typical cantilever sample interaction,
which as was mentioned above is at the heart of the
detection scheme employed by AFM's. The objective
is to ensure good performance of the microscope by
identifying and subsequently eliminating the possibil-
ity of chaotic motion of the cantilever. In this work,
we show that based on a certain model approxima-
tion of the cantilever-sample system it is possible to
design controllers that will substantially improve the
behaviour of the system by eliminating the possibility
of chaos.

2. Model Description

In Figure 1 the cantilever is modeled as a single
spring-mass system with the stiffness of the spring
being k and the equivalent mass m. The cantilever
interacts with the sample via a tip that is mounted
on the cantilever. The cantilever-tip-sample system is
modeled by a sphere of radius R and mass m, which
is suspended by a spring of stiffness k. We will fre-
quently refer to the mass m as being the tip of the
cantilever.

The tip-sample interaction is modeled by an interac-
tion potential which is given by

$$-\frac{AR}{6(Z+x)},$$

where, Z is the equilibrium position of the tip mea-
sured from a reference where the sample is positioned
in the absence of the sample, x is the displacement
of the tip measured from this equilibrium position
with the upward direction as the positive direction.
$A = \pi^2 Q \rho_1 \rho_2$ is the Hamaker constant, where Q is the
interaction constant (aqueous solute concentration in
mole fraction units (mol dm^{-3}/55.5)) [4], and ρ_1 and
ρ_2 are the densities of the tip and sample materials,
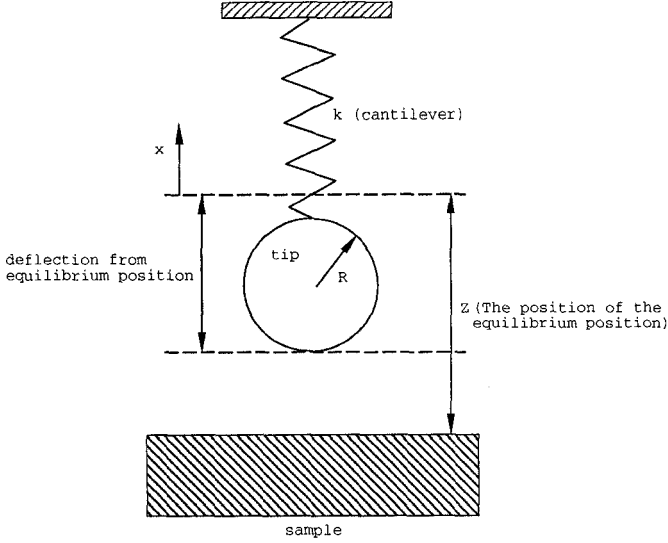respectively. Thus, the potential for the tip-sample

Figure 1: Tip-sample model.

assembly is given by

$$V(x, Z) = -\frac{AR}{6(Z+x)} + \frac{1}{2}kx^2.$$

The net energy of the system scaled by the effective mass m of the cantilever is given by $H(x, \dot{x}, Z)$ with

$$H(x, \dot{x}, Z) = \frac{1}{2}\dot{x}^2 + \frac{1}{2}\omega_1^2 x^2 - \frac{D\omega_1^2}{(Z+x)},$$

where, $\omega_1 = \sqrt{\frac{k}{m}}$ is the first modal frequency of the system and $D = \frac{AR}{6k}$. Note that H is the Hamiltonian of the system, and therefore is a constant of the dynamics (invariant of motion) since there is no dissipation.

Let $x_1 = x$ and $x_2 = \dot{x}$. The dynamics of the tip-sample system derived from the above Hamiltonian is given below ($\dot{x}_1 = \frac{\partial H}{\partial x_2}$ and $\dot{x}_2 = -\frac{\partial H}{\partial x_1}$)

$$\dot{x}_1 = x_2 \quad (1)$$

$$\dot{x}_2 = -\omega_1^2 x_1 - \frac{D\omega_1^2}{(Z+x_1)^2}. \quad (2)$$

The actual system is both damped and forced, and therefore it is not Hamiltonian. We assume that the damping and external forcing are small enough so that we can think of the actual system as a perturbed Hamiltonian system. Hence, the study of the Hamiltonian (unperturbed) system is very important, as the trajectories of this system will be used (as we will see later) to study the behaviour of the perturbed system.

If $x > 0$ then the spring force and the vdW force both are directed towards the sample and therefore

there will be no fixed points in this region. If $x < 0$ the spring force and the vdW force are directed in opposite directions and therefore there is a possibility of fixed points. However, if Z is small enough, the system will not have fixed points because the vdW force will be larger than the spring force for $x < 0$. In this case, the sample snaps the tip into contact.

Next, we find the critical value of Z below which snapping occurs. We will also show that if Z is larger than this critical value then we have two fixed points above the sample.

In order to find the fixed points of the system we set $\dot{x}_1$ and $\dot{x}_2$ to zero in equations (1) and (2). $\dot{x}_1 = 0$ implies that $x_2 = 0$, and $\dot{x}_2 = 0$ gives

$$x_1^3 + Bx_1^2 + Cx_1 + D = 0, \quad (3)$$

where, $B = 2Z$ and $C = Z^2$. We will find the roots of this polynomial as a function of Z and D. Define

$$p = C - \frac{B^2}{3} = -\frac{Z^2}{3}, \quad (4)$$

$$q = D - \frac{BC}{3} + \frac{2B^3}{27} = D - \frac{2Z^3}{27}, \text{ and } \quad (5)$$

$$R_r = \frac{p^3}{27} + \frac{q^2}{4} = \left(\frac{D}{2}\right)^2 - \frac{1}{27}DZ^3. \quad (6)$$

Let $y^3 = -\frac{q}{2} \pm \sqrt{R_r}$ and the three cube roots of y^3 be y_i, $i = 1, 2, 3$. Then the three roots of (3); x_{1i}, $i = 1, 2, 3$ are given by

$$x_{1i} = y_i - \frac{p}{3y_i} - \frac{B}{3}, \quad i = 1, 2, 3. \quad (7)$$

If $R_r < 0$ then y^3 is imaginary, otherwise it is real. Let Z_s be the solution to $R_r = 0$, i.e., the solution to

$$\left(\frac{D}{2}\right)^2 - \frac{1}{27}DZ_s^3 = 0,$$

which implies that

$$Z_s = \frac{3}{2}(2D)^{\frac{1}{3}}.$$

We divide the analysis of the dynamics into two cases; $Z \geq Z_s$ and $Z < Z_s$.

3. Dynamical Analysis: The Case $Z \geq Z_s$

In this section we discuss the important case when $Z \geq Z_s$, and at the end of the section we give a comment concerning the other case. First we analyze the system when there is no damping and forcing which will form the basis for the study of the perturbed system where the cantilever is forced sinusoidally and damping is present.

If $Z > Z_s$, $R_r < 0$ and y^3 is imaginary, we can write

$$y^3 = -\frac{q}{2} \pm j\sqrt{-R_r} = r^3 e^{\pm j\theta}, \qquad (8)$$

where,

$$r^3 = \sqrt{\frac{q^2}{4} - R_r} \qquad (9)$$

and

$$\theta = \arctan \frac{\sqrt{-R_r}}{-q/2}. \qquad (10)$$

We consider only $+j\theta$ because (as we will see later) $-j\theta$ gives the same results. Thus, the three roots of y^3 are $y_i = re^{j\theta_i}$, where, $\theta_1 = \frac{\theta}{3}$, $\theta_2 = \theta_1 + \frac{2\pi}{3}$, and $\theta_3 = \theta_1 + \frac{4\pi}{3}$. Therefore, we have

$$
\begin{aligned}
x_{1i} &= re^{j\theta_i} - \frac{p}{3r}e^{-j\theta_i} - \frac{B}{3} \\
&= \left(r - \frac{p}{3r}\right)\cos\theta_i - \frac{B}{3} + j\sin\theta_i\left(r + \frac{p}{3r}\right),
\end{aligned}
$$

for $i = 1, 2, 3$. Note that

$$r^3 = \sqrt{\frac{q^2}{4} - R_r} = \sqrt{-\frac{p^3}{27}} = \frac{Z^3}{27}.$$

Therefore, $r = Z/3$ and we get

$$r + \frac{p}{3r} = \frac{Z}{3} - \frac{-Z^2/3}{Z} = 0 \ (Z > 0).$$

Thus, the roots of (3) are real for $Z > Z_s$ and they are given by

$$x_{1i} = -\frac{2Z}{3}(1 - \cos\theta_i). \qquad (11)$$

Note that θ_i appears in the expression above only as $\cos\theta_i$ which is an even function of θ_i. Therefore, in (8) we can restrict the analysis to the roots of $y^3 = r^3 e^{j\theta}$. Thus, the fixed points for the system when $Z > Z_s$ are given by

$$(x_{1i}, 0), \ i = 1, 2, 3, \qquad (12)$$

where, x_{1i}, $i = 1, 2, 3$ are given by (11).

At the fixed point, the vdW force $\frac{mD\omega_1^2}{(Z+x_1)^2}$ and the spring force kx_1 must be equal in magnitude and opposite in direction. In other words, for a fixed point to exist at $(x_1, 0)$ the following relation must hold

$$-kx_1 = \frac{mD\omega_1^2}{(Z + x_1)^2}.$$

In Figure 2 the vdW forces for $Z = Z_s$, $Z = Z_1 < Z_s$, $Z = Z_2 > Z_s$, and $Z = Z_3 > Z_2$, and the spring force are plotted against x_1. The tip positions corresponding to the fixed points are the intersection points of the vdW and spring forces.
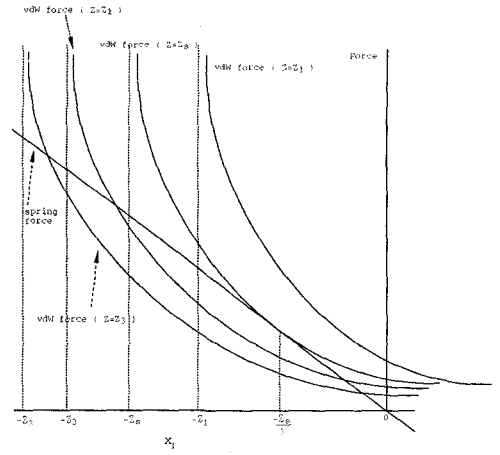

Figure 2: This figure shows the vdW force for different values of Z. The spring force is also plotted.

Note that when $Z = Z_s$, $R_r = 0$ and from equations (9) and (10) we have that $\theta = \pi$ (since $-q/2$ is negative in this case). Thus, $\theta_1 = \frac{\pi}{3}$, $\theta_2 = \pi$, and $\theta_3 = \frac{5\pi}{3}$. Therefore, $x_{11} = -\frac{Z_s}{3}$, $x_{12} = -\frac{4Z_s}{3}$, and $x_{13} = -\frac{Z_s}{3}$. x_{11} and x_{13} are equal and are located above the sample. x_{12} lies below the sample and thus has no practical significance. The spring force is equal to the vdW force at only one point above the sample, namely, $-Z_s/3$. This means that the spring force is the tangent of the vdW force at the point $-Z_s/3$ (see Figure 2).

If $Z > Z_s$ then it is clear that that $\theta \in (0, \pi)$. Therefore, $\theta_1 \in (0, \frac{\pi}{3})$, $\theta_2 \in (\frac{2\pi}{3}, \pi)$, and $\theta_3 \in (\frac{4\pi}{3}, \frac{5\pi}{3})$. This implies that $x_{11} \in (-Z_s/3, 0)$, $x_{12} \in (-4Z/3, -Z)$, and $x_{13} \in (-Z, -Z_s/3)$. Thus, we have two fixed points above the sample. This is also clear from Figure 2. Note that as Z increases the points x_{11} and x_{13} move towards zero and the sample, respectively. The two roots that correspond to the equilibrium points that are located above the sample are plotted as a function of Z as shown in Figure 3. We can see that one equilibrium point moves towards zero and the other one towards the sample as Z increases.

As Z goes to ∞, θ goes to zero since $\frac{\sqrt{-R_r}}{-q/2}$ goes to zero with positive $-q/2$. Hence, x_{11} goes to zero, x_{12} goes to the sample from below, and x_{13} goes to the sample from above. There is a fixed point at zero because the vdW force is equal to zero there. Since Z goes to ∞, the spring force is larger than the vdW force at any point between the sample and $x_{11} = 0$. When the tip gets closer to the sample the vdW force increases rapidly and it becomes equal to the spring force at a point that approaches the sample (see Figure 2).
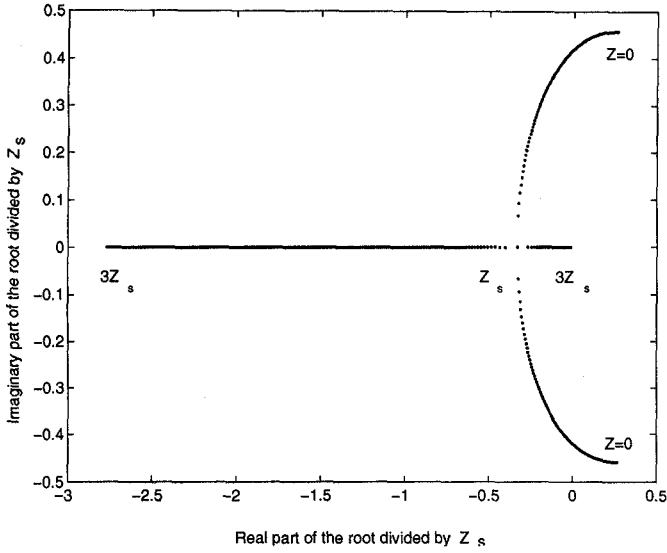
Figure 3: Root locus plot of the roots of (3) that correspond to the two fixed points above the sample as a function of Z.

3.1. Phase Portrait

We will examine the nature of the fixed points by linearizing the system as given below

$$\begin{pmatrix} \dot{x}_1 \\ \dot{x}_2 \end{pmatrix} = \begin{pmatrix} 0 & 1 \\ -\omega_1^2 + \frac{2D\omega_1^2}{(Z+x_{1i})^3} & 0 \end{pmatrix} \begin{pmatrix} x_1 \\ x_2 \end{pmatrix}, \quad i = 1, 3.$$

For $Z > Z_s$ the eigenvalues of the linearized system are purely imaginary at $x_1 = x_{11}$, and real with equal magnitude and opposite sign at $x_1 = x_{13}$. Thus, the fixed point x_{11} is a center, whereas x_{13} is a saddle point. From now on, we will denote x_{11} and x_{13} by x_c and x_s, respectively.

Figure 4 shows the phase portrait of the system. There is a homoclinic orbit connected to itself at the point $(x_s, 0)$. This homoclinic orbit is filled with periodic orbits around the the center $(x_c, 0)$. When $x_1 < x_s$ the tip accelerates towards the sample and hits it with a large velocity (snapping). Denote the maximum position on the x_1 axis that the homoclinic orbit obtains by x_e. If $x_s < x_1 < x_e$ and x_2 is not too large, the tip oscillates around the center. If x_2 is large enough, then the tip will have extra energy, so it will pass x_s accelerating towards the sample.

3.2. Homoclinic Solution

In this subsection, we find an analytic relation between time and x_1 for the homoclinic orbit. Since the Hamiltonian of the system is an invariant of motion, it is constant along the trajectories of the system. Thus, the homoclinic solution satisfies the following equation
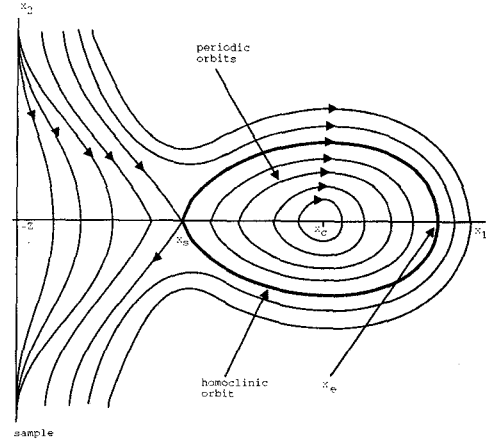
$$H(x_1, x_2, Z) = H(x_s, 0, Z).$$

Figure 4: Phase portrait.

If we let $c = H(x_s, 0, Z)$, we have

$$\frac{1}{2}x_2^2 + \frac{1}{2}\omega_1^2 x_1^2 - \frac{D\omega_1^2}{(Z+x_1)} = c.$$

This can be written as

$$x_2^2 = -\omega_1^2 \frac{x_1^3 + Zx_1^2 - \frac{2c}{\omega_1^2}x_1 - 2\left(D + \frac{c}{\omega_1^2}Z\right)}{Z + x_1}. \quad (13)$$

The roots of the numerator of the right hand side of this expression are x_s (two repeated roots) and x_e. This is because the homoclinic orbit crosses the x_1 axis at the points x_s and x_e (see Figure 4). Since for $H(x_1, x_2, Z) = c$, the solution exits on both sides of the saddle point (since x_s has stable and unstable manifolds), x_s has to be a repeated root so that x_2^2 is positive around x_s. Therefore, we have

$$\dot{x}_1 = x_2 = \pm\omega_1 (x_1 - x_s) \sqrt{\frac{x_e - x_1}{Z + x_1}}, \quad (x_s \le x_1 \le x_e).$$
$$(14)$$

Rearranging (14) and integrating, we get

$$-\sqrt{\frac{Z + x_s}{-Z - 3x_s}} \ln\left(-\frac{f_1 + f_2 + f_3}{x_s(x_1 - x_s)}\right) - \frac{\pi}{2}$$
$$- \arcsin\frac{x_1 + Z + x_s}{x_s} = \pm\omega_1 (t - t_0), \quad (15)$$

and $x_2(t)$ is obtained from (14), where, $f_1 = (Z + x_s)(-Z - 3x_s)$, $f_2 = (-Z - 2x_s)(x_1 - x_s)$ and $f_3 = \sqrt{(Z + x_s)(x_e - x_s)P}$. It was assumed that the time origin t_0 is chosen so that $x_1(t_0) = x_e$. The plus and minus signs are for $t < t_0$ and $t > t_0$, respectively. Note that for a given x_1 in the desired range of interest $x_2(-\tau) = -x_2(\tau)$ for $\tau = t - t_0$. Therefore, x_2 is an odd function of τ. Thus, we have obtained a complete description of the homoclinic orbit.

3.3. The Perturbed System

In most AFMs the cantilever motion is damped due to the surrounding air. In addition, the cantilever is

forced by a small sinusoidal signal $mf \cos \omega t$, where, ω takes values around the natural frequency ω_1 of the system. The differential equation for the perturbed system can be written as

$$\dot{x}_1 = x_2$$
$$\dot{x}_2 = -\omega_1^2 x_1 - \frac{D\omega_1^2}{(Z+x)^2} + f \cos \omega t - \mu x_2,$$

where we have assumed that the damping force per unit mass is μx_2. Given a small enough ϵ, define γ and δ such that $\epsilon \gamma = f$ and $\epsilon \delta = \mu$. Using suspension (i.e, consider the time to be a new state variable, ϕ), we have

$$\dot{x}_1 = x_2$$
$$\dot{x}_2 = -\omega_1^2 x_1 - \frac{D\omega_1^2}{(Z+x)^2} + \epsilon \left(\gamma \cos \phi - \delta x_2 \right)$$
$$\dot{\phi} = \omega,$$

where, $\phi(t) = \omega t + t_0$. Define

$$g(x_1, x_2, \phi) = \begin{pmatrix} 0 \\ \gamma \cos \phi - \delta x_2 \end{pmatrix}.$$

Thus, the Hamiltonian system described previously is now perturbed by ϵg. The next step is to study the dynamics of the perturbed system. To achieve this goal, we will study the Melnikov function for the perturbed system.

3.4. Melnikov Function
Since the system that we are considering is a time-periodic perturbation of a Hamiltonian system, Melnikov's method can be used to describe how the homoclinic orbit breaks up in the presence of the perturbation. The Melnikov function is defined as [1]

$$M(t_0, \phi_0) = \int_{-\infty}^{\infty} DH(x_{1h}(\tau), x_{2h}(\tau)) \cdot$$
$$g(x_{1h}(\tau), x_{2h}(\tau), \phi(\tau + t_0))d\tau,$$

where, $DH(x_1, x_2) = \left(\frac{\partial H}{\partial x_1} \quad \frac{\partial H}{\partial x_2} \right)$, and $x_{1h}(\tau)$ and $x_{2h}(\tau)$ are the homoclinic solution as given in subsection 3.2. Therefore,

$$M(t_0, \phi_0) = \int_{-\infty}^{\infty} x_{2h}(\tau)(\gamma \cos(\omega\tau + \omega t_0 + \phi_0) - \delta x_{2h}(\tau))d\tau.$$

After some calculations we get

$$M(t_0, \phi_0) = a_d \delta + a_s \gamma \sin(\omega t_0 + \phi_0), \quad (16)$$

where, $\quad a_d \quad = \quad -2 \int_0^{\infty} x_{2h}^2(\tau)d\tau \quad$ and $a_s = -2 \int_0^{\infty} x_{2h}(\tau) \sin \omega \tau d\tau.$

The Melnikov function is a signed measure of the distance between the stable and unstable manifolds

for the perturbed system. The manifolds intersect if the Melnikov function has zeros. The intersection of manifolds indicates the presence of chaos [1]. The Melnikov function will have zeros if and only if

$$\frac{\delta}{\gamma} \leq \left| \frac{a_s}{a_d} \right|.$$

Define

$$\left(\frac{\delta}{\gamma} \right)_{cr} = \left| \frac{a_s}{a_d} \right|.$$

If $\frac{\delta}{\gamma} > \left(\frac{\delta}{\gamma} \right)_{cr}$ then $M(t_0, \phi_0)$ has no zeros, otherwise it does.

ϕ_0 fixes a Poincaré section, while t_0 specifies a point on the unperturbed homoclinic orbit. Every zero of the Melnikov function corresponds to an intersection (within order ϵ) of the stable and unstable manifolds [1]. Note that if $\frac{\delta}{\gamma} \leq \left(\frac{\delta}{\gamma} \right)_{cr}$ then the two manifolds intersect at an infinite number of points for every Poincaré section ϕ_0.

3.5. Qualitative Behaviour
In this subsection, we define variables which facilitate the study of the qualitative behaviour of the system. Recall that

$$\dot{x}_1 = x_2$$
$$\dot{x}_2 = -\omega_1^2 x_1 - \frac{D\omega_1^2}{(Z+x_1)^2} + \epsilon \left(\gamma \cos \omega t - \delta x_2 \right).$$

Let $T = \omega_1 t$ (time scale) and divide the left and right hand sides of the above equations by Z_s to get

$$\xi_1' = \xi_2$$
$$\xi_2' = -\xi_1 - \frac{d}{(\alpha + \xi_1)^2} + \epsilon \left(\Gamma \cos \Omega T - \Delta \xi_2 \right),$$

where, $\xi_1 = \frac{x_1}{Z_s}$, $\xi_2 = \frac{x_2}{\omega_1 Z_s}$, $d = \frac{4}{27}$, $\Gamma = \frac{\gamma}{\omega_1^2 Z_s}$, $\Delta = \frac{\delta}{\omega_1}$, $\alpha = \frac{Z}{Z_s}$, and $\Omega = \frac{\omega}{\omega_1}$. The prime denotes the derivative with respect to T. In the new co-ordinates there is no explicit dependence on D and ω_1 (note that the same γ and δ give different Γ and Δ for different values of D and ω_1). In other words, there is no explicit dependence on the material properties and the dimensions of the cantilever and tip. The quantitative results differ by scaling factors depending on these two parameters.

The new system looks like the old system with Z replaced by α, D by d and ω_1 by 1. Hence, all of the previous analysis applies to the new system with the new factors. The Melnikov function in the new co-ordinates is

$$M(T_0, \phi_0) = A_d \Delta + A_s \Gamma \sin(\Omega T_0 + \phi_0),$$

where, $A_d = -2\int_0^\infty \xi_{2h}^2(\tau)d\tau$, and $A_s = -2\int_0^\infty \xi_{2h}(\tau)\sin\Omega\tau d\tau$. Define the critical value of $\frac{\Delta}{\Gamma}$ as $\left(\frac{\Delta}{\Gamma}\right)_{cr} = \left|\frac{A_s}{A_d}\right|$. It is easy to verify that

$$\left(\frac{\delta}{\gamma}\right)_{cr} = \frac{1}{\omega_1 Z_s}\left(\frac{\Delta}{\Gamma}\right)_{cr}.$$

$\left(\frac{\Delta}{\Gamma}\right)_{cr}$ is computed numerically for different values of $\alpha > 1$ and Ω around 1. The results are plotted as shown in Figure 5. If the material properties and dimensions of the cantilever and tip are given, then we first compute Z_s and ω_1 and then with the appropriate scaling transform Figure 5 to a figure with $\frac{\delta}{\gamma}$, Z, and ω as co-ordinates.

Intersection of the stable and the unstable manifolds occurs for points which lie below the surface plotted in Figure 5. As α increases the system tends to the spring-mass-damper system behaviour which does not exhibit chaotic motion when it is perturbed by a sinusoidal external forcing, and the exact trajectories of the system can be found analytically. When Z is small enough,i.e., α is close enough to 1, again there will be no chaotic motion because x_s and x_e get close enough to each other such that small perturbations cause the motion to be outside the homoclinic orbit and the sample will snap the tip into contact. If we fix α then as Ω increases the chance for chaos decreases.
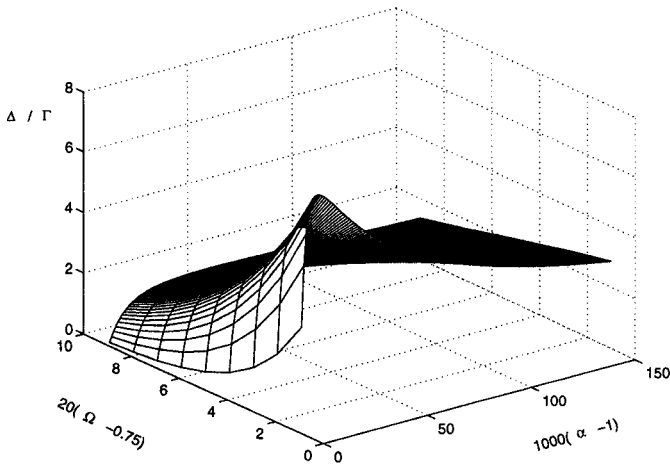

Figure 5: $\left(\frac{\Delta}{\Gamma}\right)_{cr}$ surface. The region below the surface is the region where chaos exists in the system. The region above the surface is the region of no chaos.

3.6. State Feedback Control

In most AFMs the state x_1 (position) is measured, and the state x_2 (velocity) can be estimated. This makes it possible to apply a force of the form $u =$

$k_p x_1 + k_v x_2$ to the cantilever. In this case, the state equations of the system are written as

$$
\begin{aligned}
\dot{x}_1 &= x_2 \\
\dot{x}_2 &= -\omega_1^2 x_1 - \frac{D\omega_1^2}{(Z+x_1)^2} + \epsilon\left(\gamma\cos\omega t - \delta x_2\right) \\
&\quad + \frac{k_p}{m}x_1 + \frac{k_v}{m}x_2 \\
&= -\omega_{n1}^2 x_1 - \frac{D_1\omega_{n1}^2}{(Z+x_1)^2} + \epsilon\left(\gamma\cos\omega t - \delta_1 x_2\right),
\end{aligned}
$$

where, $(\omega_{n1})^2 = \frac{k_1}{m}$ with $k_1 = k - k_p$, $D_1 = \frac{AR}{6k_1}$, and $\delta_1 = \delta - \frac{1}{\epsilon}\frac{k_v}{m}$.

We can see that applying the above state feedback control is equivalent to changing k and δ in the system independently. We will restrict our analysis to the case when $k_1 > 0$ and $\delta_1 \geq 0$.
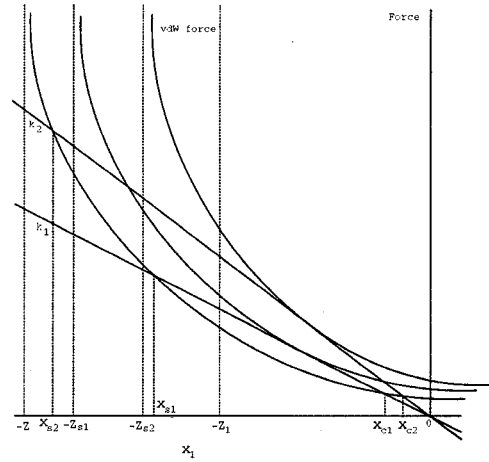

Figure 6: Spring and vdW forces.

Since k_1 and δ_1 are independent, we will discuss the effect of changing each one separately. We assume that ω, γ and Z are fixed. Suppose that $k_2 > k_1 > 0$. Then it is easy to see from Figure 6 that $-Z < x_{s2} < x_{s1}$, $0 > x_{c2} > x_{c1}$ and $Z_{s2} < Z_{s1}$. A stiffer spring allows the tip to get closer to the sample before snapping occurs, and it shifts x_c closer to zero. It is clear that the homoclinic orbits for k_1 and k_2 do not intersect.

Now by fixing $k = k_0$ and $\delta = \delta_0$ we get the point $\left(\alpha_0, \Omega_0, \left(\frac{\Delta}{\Gamma}\right)_0\right)$ in a three dimensional space, where $\alpha_0 = \frac{Z}{Z_{s0}}$ with $Z_{s0} = \frac{3}{2}\left(2\frac{AR}{6k_0}\right)^{\frac{1}{3}}$, $\Omega_0 = \frac{\omega}{\omega_{10}}$ with $\omega_{10} = \sqrt{\frac{k_0}{m}}$, and $\left(\frac{\Delta}{\Gamma}\right)_0 = \omega_{10}Z_{s0}\frac{\delta_0}{\gamma}$. Let $k = \rho k_0$, where $\rho > 0$. It is easy to see that this corresponds to the point $\left(\rho^{\frac{1}{3}}\alpha_0, \rho^{\frac{-1}{2}}\Omega_0, \rho^{\frac{1}{6}}\left(\frac{\Delta}{\Gamma}\right)_0\right)$. Varying ρ is equivalent to varying k. The variation of ρ induces a variation of the point $\left(\rho^{\frac{1}{3}}\alpha_0, \rho^{\frac{-1}{2}}\Omega_0, \rho^{\frac{1}{6}}\left(\frac{\Delta}{\Gamma}\right)_0\right)$ on a

one dimensional curve in a three dimensional space. Each curve is characterized by a fixed ω, γ, Z, and δ, and each point on the curve corresponds to a particular k. As k increases the point moves in the $+\alpha$, $-\Omega$, $+\frac{\Delta}{\Gamma}$ direction, and vice versa. Figure 7 shows curves of constant ω, γ, Z, and δ along with the $\left(\frac{\Delta}{\Gamma}\right)_{cr}$ surface. Recall that when the operating point is on or under this surface the stable and unstable manifolds intersect, otherwise they do not. If the curve of constant ω, γ, Z, and δ intersects the $\left(\frac{\Delta}{\Gamma}\right)_{cr}$ surface, then we can move the operating point from one side of this surface to the other by changing k appropriately. Note that by varying k the $\left(\frac{\delta}{\gamma}\right)_{cr}$ surface shifts in the Z, ω and $\frac{\delta}{\gamma}$ co-ordinates, while it is fixed in the α, Ω and $\frac{\Delta}{\Gamma}$ co-ordinates. Clearly, with the aid of this diagram we can select the controller parameter k_p to suppress the possibility of chaos.

Now we will analyze the effect of the controller term k_v. Let $k = k_0$ be a fixed constant and let $\delta = \rho \delta_0$. These nominal conditions give the point $(\alpha_0, \Omega_0, \rho \left(\frac{\Delta}{\Gamma}\right)_0)$. By varying ρ (δ) the operating point moves in the vertical $(\frac{\Delta}{\Gamma})$ direction . As δ increases the operating point moves in the $+\frac{\Delta}{\Gamma}$, and vice versa. Thus, we can move the operating point from one side of the $\left(\frac{\Delta}{\Gamma}\right)_{cr}$ surface to the other by changing δ appropriately. This procedure gives us the controller term k_v which results in the elimination of the possibility of chaos.

In summary, the tools of Melnikov theory are used to provide a procedure for the design of a controller of the form $u = k_v x_1 + k_p x_2$ that will eliminate chaos if it exists when $u = 0$.
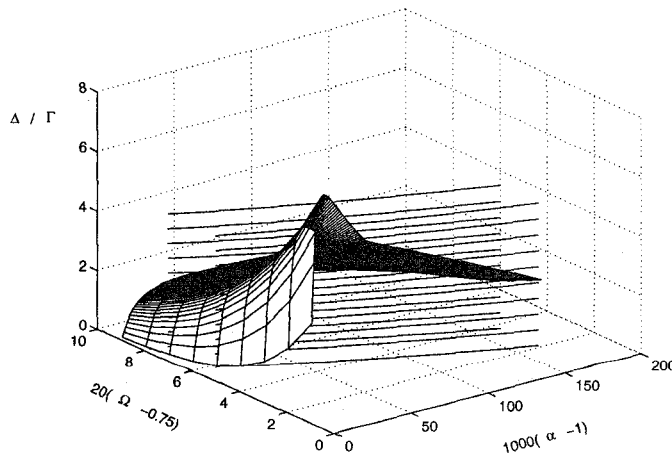

Figure 7: Curves of constant ω, γ, Z, and δ and the $\left(\frac{\Delta}{\Gamma}\right)_{cr}$ surface.

Finally, for the case when $Z = Z_1 < Z_s$, the vdW force is greater than the spring force whenever $x_1 <$

0 (see Figure 2). Hence, there are no fixed points above the sample and the corresponding two roots are imaginary as shown in Figure 3. In this case, the sample snaps the tip into contact.

4. Conclusions

A mathematical model for the cantilever-sample interaction in the AFM was utilized to explore the dynamical behaviour of the cantilever. It is shown that it is possible for chaos to exist in the system depending on the extent of damping and forcing. The region in which chaos exists was found. It was shown that feedback control can be used to eliminate the possibility of chaos. Ongoing research involves the experimental validation of the predictions, and the implementation of control to eliminate chaos.

References
[1]   Stephen Wiggins, Introduction to Applied Nonlinear Dynamical Systems and Chaos, Springer-Verlag, 1990.

[2]   Jeffrey L.Hutter and John Bechhoefer, "Calibration of atomic-force microscope tips", *Rev. Sci. Instrum.* 64(7), pp. 1868-1873, July 1993.

[3]   I. S. Gradshteyn/I. M. Ryzhik, Table of Integrals, Series, and Products, Academic Press, Inc., 1980.

[4]   Jacob N. Israelachvili, Intermolecular and Surface Forces, Academic Press, 1985.

[5]   Dror Sarid, *Scanning Force Microscopy,* Oxford University Press, New York, 1994.

[6]   N. A. Burnham, A. J. Kulik, G. Gremaud, and G. A. D. Briggs, "Nanosubharmonics: The Dynamics of Small Nonlinear Contacts", *Physical Rev. Lett.* , Vol. 74, pp 5092-5059, June 1995.